

ACCOUNTING FOR THE SPECTRAL RESOLUTION ON SIF RETRIEVAL FROM A NARROW-BAND AIRBORNE IMAGER USING SCOPE

A. Belwalkar¹, T. Poblete¹, A. Hornero^{1,3,4}, P.J. Zarco-Tejada^{1,2,3}

¹Department of Infrastructure Engineering, Faculty of Engineering and Information Technology (FEIT), The University of Melbourne, Melbourne, Victoria, Australia

²School of Agriculture and Food, Faculty of Veterinary and Agricultural Sciences (FVAS), The University of Melbourne, Melbourne, Victoria, Australia

³Instituto de Agricultura Sostenible (IAS), Consejo Superior de Investigaciones Científicas (CSIC), Alameda del Obispo s/n, 14004 Córdoba, Spain

⁴Department of Geography, Swansea University, SA2 8PP Swansea, United Kingdom

ABSTRACT

Sub-nanometer hyperspectral imagers are increasingly being used to quantify solar-induced chlorophyll fluorescence (SIF) due to their ability to characterize narrow absorption features accurately. However, some limitations prevent their wide use in the operational context due to their high cost, weight, and complexity. On the other hand, more widely-used narrow-band hyperspectral imagers with 4–6 nm full width at half-maximum (FWHM) resolution could be a cost-effective alternative for acquiring high-spatial-resolution hyperspectral imagery to derive SIF. Due to the large effects of the spectral resolution (SR) on the quantified fluorescence, the SIF levels derived from such airborne imagers with 4–6 nm FWHM are overestimated, requiring careful interpretation. In this study, we flew in tandem two airborne hyperspectral imagers with different spectral characteristics. These sensors' imagery was used to model the impact of SR on the SIF quantification using the Soil-Canopy Observation of Photosynthesis and Energy (SCOPE) model. A Support Vector Machine regression (SVR) model trained via SCOPE simulations was employed to quantify SIF at 1 nm SR from the original 5.8 nm FWHM resolution. The performance of the SIF quantification was evaluated theoretically with SCOPE and tested against airborne hyperspectral radiance and the derived SIF. Results showed that the estimated SIF at 1 nm SR agreed well with the reference SCOPE simulations (RMSE=0.097 mW/m²/nm/sr) and with airborne-quantified SIF (RMSE=0.094 mW/m²/nm/sr).

Index Terms— Airborne, hyperspectral, SIF, 3FLD, solar-induced fluorescence, SCOPE, radiative transfer.

1. INTRODUCTION

The quantification of SIF using imaging sensors onboard airborne platforms has made significant progress in the last decade. SR has improved from narrow-band hyperspectral imagers (i.e., 4–6 nm FWHM) to sub-nanometer sensors specifically designed for accurate SIF retrievals [1]. These airborne imaging spectroscopy sensors provide spatial patterns of fluorescence across the landscape, enabling the development of indicators of photosynthetic functioning used for pre-visual vegetation stress [2], [3]. Although SIF quantification in absolute physical units requires sub-nanometer resolutions [1], the availability of airborne imaging sensors with such capabilities is limited due to their high cost and operational complexity. On the other hand, narrow-band imaging sensors characterized by spectral resolutions ranging from 4–6 nm FWHM are widely available. They can be installed onboard lightweight platforms for operational SIF retrievals needed in precision agriculture applications. Previous studies [4]–[6] have demonstrated the relevance of retrieving SIF from narrow-band sensors in the context of plant physiology, and particularly for the pre-visual detection of biotic and abiotic stress. Recent research [7] found that SIF estimates derived from a narrow-band hyperspectral imager with a 5.8 nm FWHM correlated strongly with ground-based and sub-nanometer airborne SIF estimates acquired simultaneously. However, such narrow-band SIF estimates are overestimated, and their correct interpretation is critical, particularly in applications of plant phenotyping and precision agriculture. Therefore, work is needed to develop methods based on radiative transfer models (RTMs) to accurately quantify SIF from narrow-band hyperspectral imagers.

Light re-absorption and scattering within the canopy, which is driven by vegetation structure and plant pigments, have a

strong influence on the top of canopy (TOC) SIF [8], [9]. Global sensitivity analyses using SCOPE [10] identified leaf chlorophyll content (C_{a+b}), leaf area index (LAI), and the leaf inclination distribution parameter ($LIDF_a$) as key variables driving the majority of SIF variability [11]. The current study makes progress on the development of modelling methods that account for the spectral resolution when estimating SIF at 1 nm resolution from narrow-band hyperspectral imagery. Leaf biochemistry and structural traits derived from SCOPE model inversions were used as inputs in a modelling approach to assess their impact on the SIF estimates obtained from a narrow-band imager. Sub-nanometer imagery collected concurrently was used for validation purposes to assess the model performance.

2. MATERIALS AND METHODS

2.1. Experimental and simulated datasets

2.1.1. Airborne hyperspectral imagery

On 9 October 2019 an airborne campaign was conducted over a field trial site in Yarrowonga (36°02'55"S, 145°59'02"E), Australia, under clear sky conditions. Several varieties of dryland wheat were grown under varying physiological conditions induced by a range of nitrogen fertilizer application rates. A narrow-band hyperspectral imager (Hyperspec VNIR E-Series model, Headwall Photonics, Fitchburg, MA, USA) in the 400–1000 nm spectral region with 5.8 nm FWHM resolution and a sub-nanometer hyperspectral imager (Hyperspec Fluorescence sensor, Headwall Photonics, Fitchburg, MA, USA) in the 670–780 nm spectral region with 0.1–0.2 nm FWHM were installed in tandem on a Cessna 172R aircraft operated by the HyperSens Laboratory, University of Melbourne's Airborne Remote Sensing Facility. The total incoming irradiance was measured with a 0.065-nm FWHM HR-2000 spectrometer (Ocean Insight, Dunedin, FL, USA) equipped with a CC-3 VIS-NIR cosine corrector diffuser. Mean radiance spectra corresponding to both hyperspectral imagers and reflectance spectra from the narrow-band hyperspectral imager were extracted from pure vegetation pixels identified within individual plots. Radiance and reflectance spectra were used to quantify SIF and estimate plant traits by radiative transfer, respectively (Fig. 1). A full description of the airborne campaign, data preprocessing and image correction can be found in Belwalkar *et al.* [7].

2.1.2. SCOPE model simulations

Simulations were carried out using the SCOPE model (version 2.0), which integrates three radiative transfer modules and an energy balance module to estimate outgoing radiation spectra, reflectance and chlorophyll fluorescence [10]. A training dataset of 10,000 simulations and a test dataset of 1,000 simulations were generated independently by randomly varying specific input parameters drawn from a

uniform distribution. The following ranges were set based on field measurements and from the existing literature: C_{a+b} [10–70] $\mu\text{g}/\text{cm}^2$, LAI [0.5–5] m^2/m^2 , $LIDF_a$ [-1 to 1], leaf carotenoid content (C_{x+c}) [1–20] $\mu\text{g}/\text{cm}^2$, leaf anthocyanins content (Anth.) [0–8] $\mu\text{g}/\text{cm}^2$, leaf dry matter content (C_{dm}) [0.001–0.05] g/cm^2 , leaf water content (C_w) [0.001–0.05] cm, leaf structure parameter (N) [1–1.5], maximum carboxylation capacity ($V_{c_{mo}}$) [30–110], and the bimodality of the leaf angle distribution ($LIDF_b$) as 0. All other SCOPE input parameters were left at their default settings. The air temperature and air pressure inputs were obtained from a portable weather station during the airborne campaign at the field trial site. The TOC spectra of total upwelling radiance, reflectance, SIF radiance, and corresponding irradiance were simulated for each case using SCOPE at the default 1.0-nm SR and 1.0-nm spectral sampling interval (SSI). All simulations were convolved to the narrow-band hyperspectral imager's wavelength range, SSI, and SR assuming a gaussian band spectral response function.

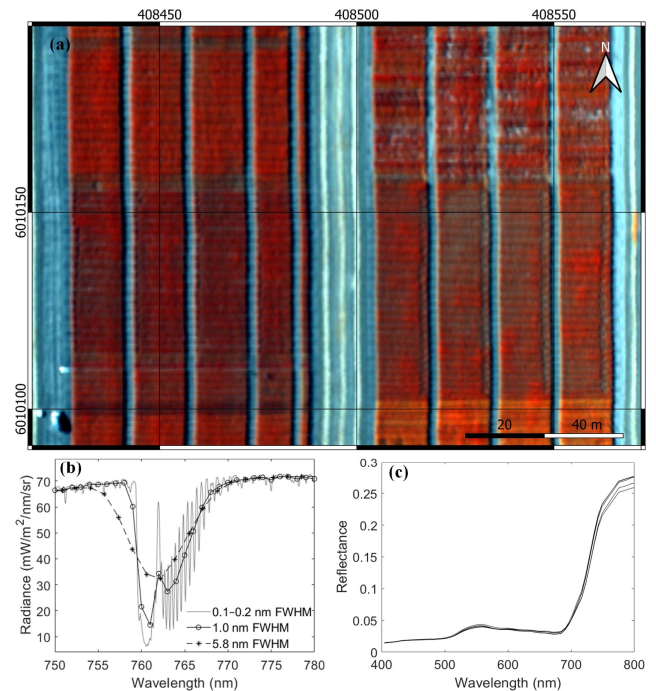


Fig. 1: Airborne hyperspectral image acquired over the field trial site. Airborne radiance (b) and reflectance (c) were used for SIF quantification and plant traits estimation using SCOPE model inversions. The 1.0 nm FWHM radiance shown in (b) were obtained by convolving the original sub-nanometer resolution (0.1–0.2 nm FWHM) spectra.

2.2. SIF quantification and inversion of plant traits

The radiance spectra extracted from the sub-nanometer imager were convolved to the default 1.0-nm SR and 1.0-nm SSI used in SCOPE (Fig. 1b). The resampled sub-nanometer-derived radiance was used to calculate the SIF

used as a reference against the SIF quantified from the narrow-band hyperspectral imager using the modelling approach proposed in this study. The O₂-A band *in-filling* approach was used to quantify SIF from both simulated and airborne datasets, employing the Fraunhofer Line Depth (FLD) principle with a total of three spectral bands (3FLD) [12]. The airborne SIF was further corrected and normalized to account for the atmospheric and directional effects, as described in Belwalkar *et al.* [7]. A look-up table with 100,000 simulations was built by randomly varying the SCOPE input parameters with a uniform distribution within the ranges described in section 2.1.2. Reflectance spectra were matched with the spectral resolution of the narrow-band hyperspectral imager. The reflectance spectra from the SCOPE simulations and the narrow-band hyperspectral imager in the 400–800 nm spectral range (Fig. 1c) were used to estimate C_{a+b}, LAI, and LIDF_a using an RTM-based hybrid inversion with random forest regression [13].

2.3. Estimation of SIF at 1 nm resolution from narrow-band airborne spectra

We evaluated two models for estimating SIF at 1 nm resolution from narrow-band 5.8 nm spectra. The slope and coefficient obtained from the linear relationship between 3FLD retrievals at 1 nm and 5.8 nm from the SCOPE simulated training dataset were used to scale narrow-band SIF retrievals to 1 nm SR in the first model, named here as the linear model. The second model was based on an SVR built using the simulated training dataset, with i) narrow-band SIF quantified using the 3FLD method, and ii) SCOPE-derived C_{a+b}, LAI, and LIDF_a as inputs. The SVR model was first trained in parallel (MATLAB parallel computing toolbox) using a radial basis function and optimizing the hyperparameters during training to predict SIF at 1 nm SR. A 10-fold cross-validation strategy was employed to avoid overfitting on the training samples.

The performance of both models was evaluated using root mean square error (RMSE) and normalized root mean square error (nRMSE) as metrics. The estimated SIF from the simulated test dataset was compared against the reference SCOPE modelled SIF. Additionally, both models were evaluated on the airborne datasets to test the applicability of the models on the experimental data. The SCOPE-based hybrid inversion retrieved the three leaf biochemistry and structural traits. Airborne SIF estimated at 1 nm FWHM from the 5.8 nm spectra was compared against the resampled sub-nanometer SIF, and error metrics were calculated.

3. RESULTS

Fig. 2 shows the range of variation for the leaf traits estimated from the airborne reflectance data using the

SCOPE-based hybrid inversion approach. C_{a+b} exhibited the most significant variability across the experimental plots, attributed to the changes in physiological conditions and nitrogen fertilizer application rates.

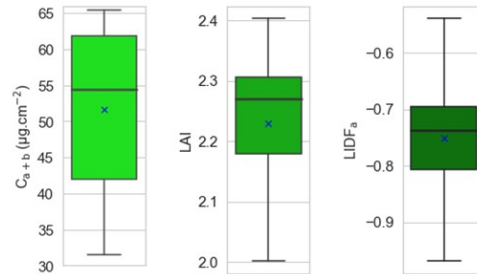


Fig. 2: Range of variation associated with C_{a+b}, LAI and LIDF_a estimated from airborne hyperspectral reflectance. The median and mean values are denoted by a black line within the box, and the marker 'x', respectively.

The predicted SIF using both linear and SVR models from SCOPE simulated data showed significant relationships with the reference 1 nm FWHM SIF ($R^2 > 0.9$, $p < 0.001$; Fig. 3a and 3b). The SVR model outperformed (nRMSE=8.82%) the linear model (nRMSE=12.16%), but the slope of the linear relationship remained close to 1 for both models.

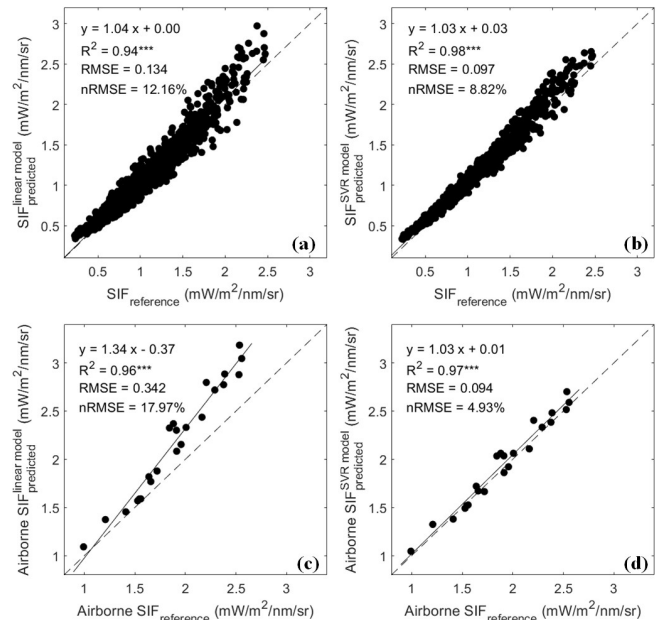


Fig. 3: Relationships between the 1 nm FWHM SIF simulated by SCOPE (used here as the reference SIF) and the SIF estimated by the linear model (a) and by the SVR model (b) from 5.8 nm FWHM spectra. Relationships between the airborne SIF quantified from the sub-nanometer imager and the airborne SIF at 1 nm FWHM estimated by the linear model (c) and SVR model (d) from the 5.8 nm narrow-band airborne spectra. * p -value <0.05 ; ** p -value <0.01 ; *** p -value <0.001 .

The linear model consistently overestimated the SIF estimated from the narrow-band airborne hyperspectral data, as expected, which was more pronounced for higher SIF values (nRMSE=17.97%, $p < 0.001$; Fig. 3c). In contrast, the predicted airborne SIF at 1 nm FWHM from the airborne 5.8 nm FWHM spectra using the SVR model demonstrated strong agreement with the sub-nanometer derived airborne SIF used as reference (nRMSE=4.93%, $p < 0.001$; Fig. 3d) and was closer to the 1:1 line.

These results suggest that the 5.8 nm FWHM SIF estimates can be scaled to 1 nm resolution using SCOPE radiative transfer modelling techniques and plant-retrieved parameters. These findings also indicate that machine learning models built with leaf and canopy biochemistry and structural traits in addition to narrow-band SIF quantification can improve the SIF retrieval to match the absolute levels of fluorescence expected at 1-nm resolution.

4. CONCLUSIONS

This study investigated the estimation of SIF at 1 nm FWHM from narrow-band airborne hyperspectral radiance collected at 5.8 nm FWHM using RTM modelling techniques. SIF predictions at 1 nm resolution were carried out with an SVR regression model using SCOPE-simulated narrow-band SIF data and leaf biochemical and canopy structural traits as inputs. The model was validated using simulated and experimental airborne SIF imagery acquired at 0.1–0.2 nm FWHM resolution. Results showed strong agreement with both simulated and experimental airborne datasets, with RMSEs lower than 0.1 $\text{mW/m}^2/\text{nm}/\text{sr}$. These findings suggest that RTM-based modelling methods applied to airborne hyperspectral imagers with >1 nm FWHM resolution, which are commonly used in precision agriculture, enable the retrieval of SIF at appropriate absolute physical levels, avoiding the overestimation typically obtained by lower spectral resolution instruments.

5. ACKNOWLEDGEMENTS

The authors would like to thank the Foundation for Arable Research Australia and Riverine Plains Incorporated for providing and managing the plot trials. A. Gracia-Romero and A. Longmire are acknowledged for their technical assistance during the field and airborne campaign.

6. REFERENCES

[1] G. H. Mohammed et al., "Remote sensing of solar-induced chlorophyll fluorescence (SIF) in vegetation: 50 years of progress," *Remote Sens. Environ.*, vol. 231, Sep. 2019.

[2] P. J. Zarco-Tejada et al., "Previsual symptoms of Xylella fastidiosa infection revealed in spectral plant-trait alterations," *Nat. Plants*, vol. 4, no. 7, pp. 432–439, Jul. 2018.

[3] U. Rascher et al., "Sun-induced fluorescence - a new probe of photosynthesis: First maps from the imaging spectrometer HyPlant," *Glob. Chang. Biol.*, vol. 21, no. 12, pp. 4673–4684, Dec. 2015.

[4] C. Panigada et al., "Fluorescence, PRI and canopy temperature for water stress detection in cereal crops," *Int. J. Appl. Earth Obs. Geoinf.*, vol. 30, no. 1, pp. 167–178, 2014.

[5] P. J. Zarco-Tejada et al., "Divergent abiotic spectral pathways unravel pathogen stress signals across species," *Nat. Comm.*, vol. 12, no. 1, Dec. 2021.

[6] A. Damm et al., "Far-red sun-induced chlorophyll fluorescence shows ecosystem-specific relationships to gross primary production: An assessment based on observational and modeling approaches," *Remote Sens. Environ.*, vol. 166, pp. 91–105, Sep. 2015.

[7] A. Belwalkar, T. Poblete, A. Longmire, A. Hornero, R. Hernandez-Clemente and P. J. Zarco-Tejada, "Evaluation of SIF retrievals from narrow-band and sub-nanometer airborne hyperspectral imagers flown in tandem: Modelling and validation in the context of plant phenotyping," *Remote Sens. Environ.*, vol. 273, May 2022.

[8] B. Dechant et al., "Canopy structure explains the relationship between photosynthesis and sun-induced chlorophyll fluorescence in crops," *Remote Sens. Environ.*, vol. 241, May 2020.

[9] Y. Zeng, G. Badgley, B. Dechant, Y. Ryu, M. Chen, and J. A. Berry, "A practical approach for estimating the escape ratio of near-infrared solar-induced chlorophyll fluorescence," *Remote Sens. Environ.*, vol. 232, Oct. 2019.

[10] C. van der Tol, W. Verhoef, J. Timmermans, A. Verhoef, and Z. Su, "An integrated model of soil-canopy spectral radiances, photosynthesis, fluorescence, temperature and energy balance," *Biogeosciences*, vol. 6, pp. 3109–3129, 2009.

[11] J. Verrelst, J. P. Rivera, C. van der Tol, F. Magnani, G. Mohammed, and J. Moreno, "Global sensitivity analysis of the SCOPE model: What drives simulated canopy-leaving sun-induced fluorescence?," *Remote Sens. Environ.*, vol. 166, pp. 8–21, Sep. 2015.

[12] J. A. Plascyk and F. C. Gabriel, "The Fraunhofer Line Discriminator MKII-An Airborne Instrument for Precise and Standardized Ecological Luminescence Measurement," *IEEE Trans. Instrum. Meas.*, vol. 24, no. 4, pp. 306–313, Dec. 1975.

[13] C. Camino et al., "Detection of Xylella fastidiosa in almond orchards by synergic use of an epidemic spread model and remotely sensed plant traits," *Remote Sens. Environ.*, vol. 260, Jul. 2021.